Stability and Folding of Dihydrofolate Reductase from the Hyperthermophilic Bacterium *Thermotoga maritima*[†,‡]

Thomas Dams[§] and Rainer Jaenicke*

Institut für Biophysik und Physikalische Biochemie, Universität Regensburg, D-93040 Regensburg, Germany

Received March 18, 1999; Revised Manuscript Received May 10, 1999

ABSTRACT: Dihydrofolate reductase (DHFR) has been a well-established model system for protein folding. The enzyme DHFR from the hyperthermophilic bacterium *Thermotoga maritima* (TmDHFR) displays distinct adaptations toward high temperatures at the level of both structure and stability. The enzyme represents an extremely stable dimer; no isolated structured monomers could be detected in equilibrium or during unfolding. The equilibrium unfolding strictly follows the two-state model for a dimer ($N_2 \rightleftharpoons 2U$), with a free energy of stabilization of $\Delta G = -142 \pm 10$ kJ/mol at 15 °C. The two-state model is applicable over the whole temperature range (5−70 °C), yielding a ΔG vs T profile with maximum stability at around 35 °C. There is no flattening of the stability profile. Instead, the enhanced thermostability is characterized by shifts toward higher overall stability and higher temperature of maximum stability. TmDHFR unfolds in a highly cooperative manner via a nativelike transition state without intermediates. The unfolding reaction is much slower (ca. 10^8 times) compared to DHFR from *Escherichia coli* (EcDHFR). In contrast to EcDHFR, no evidence for heterogeneity of the native state is detectable. Refolding proceeds via at least two intermediates and a burst-phase of rather low amplitude. Reassociation of monomeric intermediates is not rate-limiting on the folding pathway due to the high association constant of the dimer.

Protein stability is the result of a delicate balance of strong attractive and repulsive forces, yielding the free energy of stabilization as a small difference between large numbers equivalent to a few weak intermolecular interactions (*1*). In going from mesothermal to hyperthermal habitats, the thermodynamically relevant change in absolute temperature (degrees Kelvin) is relatively small; thus, just a few additional favorable interactions are sufficient for thermal adaptation to high temperatures. Using structural data alone, it is diffcult to decide which changes in a thermophilic protein are responsible for the gain in stability, compared to its mesophilic counterparts. Although several mechanisms of thermal stabilization such as clusters of salt bridges and H-bonds, extended secondary structure, improved packing, and higher states of oligomerization have been put forward, no general adaptive rules have been established yet. Evidently, small increments of additional free energy can be distributed over the whole molecule, i.e., at all levels of the structural hierarchy of proteins (*2*).

The comparison of the thermodynamics and kinetics of the reversible unfolding of proteins from mesophiles, thermophiles, and hyperthermophiles provides insight into the stability and self-organization which cannot be obtained from direct structural investigations. For example, temperature-dependent folding studies have been applied to mimic the in vivo conditions in hyperthermophiles (*3, 4*).

Due to the central position of the enzyme in the metabolism, dihydrofolate reductases (DHFRs)[1] from more than 30 species from all 3 domains of life have been characterized with respect to their structure and structure−function relationship. High-resolution crystallographic data and the enzymatic mechanism have been elaborated in great detail over the years (for references, cf. *5*). In addition, for more than a decade, DHFR has served as a model system for protein folding both in vitro (*6*−*8*) and in vivo (*9*−*12*). The wealth of information allows comparisons with respect to a wide variety of structural and functional aspects. In extending the data set toward ultrastable homologues from hyperthermophiles, one would expect that tendencies disclosed from a narrower temperature range might become more pronounced or even clearly significant.

Recently, TmDHFR from the hyperthermophilic bacterium *Thermotoga maritima* ($T_{max} = 90$ °C, $T_{opt} = 80$ °C) was purified and characterized. The enzyme was found to be the most thermostable DHFR isolated so far (*13*). In contrast to

[†] This work was supported by the Deutsche Forschungsgemeinschaft (Grant Ja78/33-3) and the Fonds der Chemischen Industrie.

[‡] Dedicated to Professor Max. F. Perutz on the occasion of his 85th birthday.

* Address correspondence to this author at Biochemie II, Universität Regensburg, D-93040 Regensburg, Germany. Phone: (49)941 943 3015. FAX: (49)941 943 2813. E-mail: rainer.jaenicke@biologie.uni-regensburg.de.

[§] Present address: Max-Planck-Institut für Biochemie, Abteilung Strukturforschung, D-82152 Martinsried, Germany.

[1] Abbreviations: $C_{1/2}$, denaturant concentration at the transition midpoint; CD, circular dichroism; [D], denaturant concentration; DHFR, dihydrofolate reductase; Ec as suffix, *Escherichia coli*; GdmCl, guanidinium chloride; HPLC, high-pressure liquid chromatography; N, native state; n.d., not determined; SDS−PAGE, sodium dodecyl sulfate−polyacrylamide gel electrophoresis; Tm as suffix, *Thermotoga maritima*; T_m, melting temperature; $T_{opt.}$, optimum temperature; U, unfolded state; UV, ultraviolet; ΔC_p, change in heat capacity; ΔG, Gibbs free energy; ΔG_{H2O}, Gibbs free energy in buffer; ΔH, change in enthaply; ΔS, change in entropy; $[\Theta]_{MRW}$, mean residue ellipticity; λ_{em}, emission wavelength; λ_{exc}, excitation wavelength.

10.1021/bi990635e CCC: $18.00
Published on Web 06/23/1999

the majority of previously described DHFRs, it forms a stable homodimer. Preliminary reports on two other dimeric homologues from mesophiles (*14*, *15*) have not been followed up by further characterization. It is tempting to attribute the high intrinsic stability of TmDHFR to the anomalous state of association (*4*, *16*). However, to differentiate between effects at the secondary and tertiary level, on one hand, and quaternary contributions, on the other, a detailed thermodynamic and kinetic analysis of the stability and folding of TmDHFR is needed.

MATERIALS AND METHODS

Protein Preparation. For the preparation of recombinant TmDHFR and enzyme assays, cf. ref *13*. Quartz bidistilled, degassed water was used throughout. Chemicals were of analytical grade. The purity of the protein was proved by analytical HPLC and SDS−PAGE. Determination of protein concentrations made use of the molar absorption coefficient of 22920 M^{-1} cm^{-1} for the dimeric enzyme. For all experiments, 10 mM potassium phosphate buffer, pH 7.8, 0.2 mM EDTA was used. Since TmDHFR does not contain cysteine, no reducing agent was required.

Spectroscopic Methods. Cuvettes were thermostated with an accuracy ±0.1 °C by Peltier elements. Absorption spectra were recorded in 1 cm cuvettes using a Varian Cary 1/3 spectrophotometer. Fluorescence emission was measured in a Spex Fluoromax-2 fluorometer: slit widths for excitation and emission, 1−5 and 3−5 nm, respectively; excitation wavelength, λ_{exc} = 280 nm. In the case of long-term measurements, photobleaching was minimized by continuous stirring and by opening the excitation shutter for only short time intervals. Cuvettes contained 3 mL volume and were tightly sealed with a Teflon stopper. To test for aggregates, the same wavelength for excitation and emission (330 nm) was used. Circular dichroism was recorded in 1 or 2 mm cuvettes using a Jasco J-715 spectropolarimeter. No photobleaching was observed during far-UV CD measurements. Native and unfolded TmDHFRs show a maximum of their absorption difference at 288 nm; therefore, in transition experiments, the exposure of tryptophan from the hydrophobic interior of the enzyme to the solvent was measured at this wavelength. To determine the number of buried Trp residues (*17*), again the change in extinction at 288 nm was used. In ref *17*, the change in extinction is given only for 292 nm ($\Delta\epsilon_{292} = -1600$ M^{-1} cm^{-1}); it was corrected to $\Delta\epsilon_{288} = -2580$ M^{-1} cm^{-1} based on the ratio of $\epsilon_{288}/\epsilon_{292}$ for tryptophan.

Analytical Ultracentrifugation. Sedimentation analysis was performed in a Beckman Model E analytical ultracentrifuge, using an AnG-rotor with double-sector cells and sapphire windows. Sedimentation velocity experiments at 44 000 rpm and 20 °C made use of synthetic boundary double-sector cells. Sedimentation coefficients, $s_{20,w}$, were calculated from log *r* vs *t* plots. To detect possible concentration-dependent association or heterogeneity, high-speed sedimentation equilibria at 16 000 and 20 000 rpm were performed, making use of the meniscus depletion technique (*18*). The partial specific volume, 0.750 cm^3 g^{-1}, was calculated from the amino acid composition. Upon unfolding, this value is decreased (*19*); as a consequence, the value for the monomer molecular mass at high denaturant concentration is slightly higher than the one calculated from the amino acid composition. Still, monomers could be clearly discriminated from dimers. Analysis of sedimentation equilibria made use of a program developed by Dr. G. Böhm (Universität Halle); association equilibria were evaluated using a program kindly provided by Prof. A. P. Minton (Bethesda, MD).

Equilibrium Studies. Dissociation and complete unfolding of TmDHFR were accomplished by incubating the enzyme at 55 °C for 2 h in the presence of 7.2 M GdmCl. For denaturation−renaturation transitions, native and unfolded TmDHFR was rapidly mixed with buffer solutions of varying denaturant concentration by quickly adding 950 μL of buffer to 50 μL of protein solution, both equilibrated at the desired temperature. Denaturant concentrations were measured by refractometry (*20*). Protein concentrations varied between 2 and 500 μg/mL. At temperatures above 50 °C, equilibration of both *unfolding and refolding* to a coinciding transition profile needed close to 1 week incubation. Below 50 °C, to reach equilibrium for the *refolding* transition took more than 1 week.

The ratio of denatured and total protein in the transition range, f_d, was calculated from their signal *Y* relative to the signal of the native and unfolded base line Y_N and Y_U:

$$f_d = (Y_N - Y)/(Y_N - Y_U) \quad (1)$$

Y_U and Y_N resulted from linear extrapolation of the pre- and post-transitional base lines:

$$Y_U = S_U + m_U[D];\ Y_N = S_N + m_N[D] \quad (2)$$

The relative population of species was transformed to the respective equilibrium constant K_u for a dimer according to (*21*)

$$K_u = 2P_t[f_d^2/(1 - f_d)] \quad (3)$$

with the monomer concentration P_t in moles per liter. To calculate free energies of stabilization

$$\Delta G = -RT \ln K \quad (4)$$

the equilibrium constant has to be normalized before taking the logarithm. Usually, standard concentrations of 1 M of all reactants are introduced (*22*); *R* is the gas constant [8.31 J/(mol·K)] and *T* is the absolute temperature. Thus, for every point in the transition region, a value for ΔG could be calculated; linear extrapolation to zero denaturant concentration then yielded the free energy of stabilization in buffer, i.e., at zero denaturant concentration, ΔG_{H2O}, as well as the cooperativity parameter *m*:

$$\Delta G = \Delta G_{H2O} + m[D] \quad (5)$$

Kinetic Studies. Time-dependent folding/unfolding measurements were followed by fluorescence emission (λ_{exc} = 280 nm, λ_{em} = 330 nm) and circular dichroism (λ = 222 nm). Manual mixing with a dead-time of 10−15 s and continuous stirring were used throughout. Protein concentrations varied between 0.1 and 5.2 μM. The final denaturant concentration was determined by refractometry. Fits of progress curves were obtained by using SigmaPlot 3.0 for

Table 1: Biophysical Parameters of Native and Unfolded TmDHFR[a]

	native	unfolded
molecular mass[b]	38 ± 2	22 ± 4
sedimentation coefficient[c] (S)	2.2 ± 0.4	0.53 ± 0.2
fluorescence: λ_{max} (nm)	335	352
CD at 222 nm: $[\Theta]_{MRW}$ (deg cm^2 dmol^{-1})	−11000	−2500

[a] Native: in 10 mM potassium phosphate buffer (pH 7.8) + 0.2 mM EDTA; unfolded: in 7.2 M GdmCl in the same buffer. [b] From high-speed sedimentation equilibria. [c] $s_{20,w}$ from sedimentation velocity.

Windows; the nonlinear fit-mode was programmed to evaluate:

$$A(t) = \sum_i A_i \exp(-\lambda_i t) + A_\infty \quad (6)$$

For unfolding, a value of $i = 1$ was sufficient; for refolding reactions in ≤1.8 M GdmCl at 15 °C (≤2.5 M GdmCl at 55 °C), the data could only be fitted setting $i = 2$. A_i is the amplitude of the respective phase i, and A_∞ is the signal of the final state. The difference between A_0, the amplitude at $t = 0$, and the spectroscopic signal obtained from the extrapolation of the pre- and post-transitional base lines (cf. eq 2) represents the dead-time amplitude; λ_i refers to the apparent rate constants of the respective phase i; in the case of irreversible reactions, it equals the rate constant k_i.

Kinetic m-values are defined by the dependence of rate constants on denaturant concentration and were determined by a linear fit of the logarithm of k vs the denaturant concentration [D]:

$$m_{kin} = -RT \frac{d \ln (k/s^{-1})}{d[D]} \quad (7)$$

where s^{-1} is introduced for normalization.

The interpretation of the kinetic data followed the Eyring formalism (*23*), defining the activated complex with the highest free energy ($\Delta G^{\ddagger}$) as an explicit thermodynamic state. Rate constants k are determined by that activated state:

$$k = (\kappa k_B T/h) \exp(-\Delta G^{\ddagger}/RT) \quad (8)$$

with κ the transmission coefficient (ususally set to unity, *24*), k_B the Boltzmann constant (1.381×10^{-23} J/K), and h the Planck constant (6.626×10^{-34} Js). Resulting $\Delta G^{\ddagger}$ values consist of the activation enthalpy ($\Delta H^{\ddagger}$), the activation entropy ($\Delta S^{\ddagger}$), and the change in heat capacity upon activation ($\Delta C^{\ddagger}_p$), referring to standard conditions (25 °C):

$$\Delta G^{\ddagger}(T) = \Delta H^{\ddagger}_{25\,°C} - T\Delta S^{\ddagger}_{25\,°C} + \Delta C^{\ddagger}_p[(T - 298\ K) - T \ln(T/298\ K)] \quad (9)$$

RESULTS

Equilibrium Transitions. Unfolding of TmDHFR is an extremely slow process requiring high concentrations of guanidinium chloride (GdmCl) to reach the unfolded state in finite time (*13*). The unfolded state is the monomer with its hydrophobic interior exposed to the solvent. No secondary structure is retained (Table 1). To quantify protein stability, the free energy of stabilization ΔG was determined from the equilibrium between the native and denatured states of the protein. Renaturation was reversible at all temperatures, yielding the dimeric, enzymatically fully active state. To achieve coincidence of the denaturation and the renaturation transitions within a finite time, temperatures beyond 50 °C had to be applied; at room temperature, the equilibration took extremely long due to strong kinetic hysteresis between the renaturation and the denaturation transitions. The midpoint of denaturation was observed at significantly higher GdmCl concentration than the midpoint of renaturation. The refolding transition showed no further change with time after 1 week at 15 °C; on the other hand, the unfolding reaction proceeded asymptotically toward the refolding curve (data not shown). Still, it was possible to extract ΔG values even for low temperatures, because the renaturation transition was found to represent the equilibrium state. Experimental evidence was gained from the following arguments: (i) Over the whole transition, no aggregation was detectable, indicating that there are no irreversible side reactions; refolding from any point along the transition was fully reversible; no decrease in the renaturation yield from intermediate denaturant concentrations occurred (*25*). Furthermore, denatured species from the hysteresis range folded back with the same kinetics compared with the established denatured state at high GdmCl concentration (cf. Figure 1B). Accordingly, any non-native species within the range of the renaturation transition must belong to the unfolded state U. (ii) Due to the high stability of TmDHFR, reaching the unfolding equilibrium is simply a matter of time; the equilibration can be enhanced by increasing the temperature. (iii) For monomeric proteins obeying the two-state model, no difference in the rates of unfolding and refolding would be expected at the transition midpoint. The observation that in the $N_2 \rightleftarrows 2U$ transition the renaturation rate exceeds the rate of denaturation, seems to contradict the two-state assumption. However, the folding of a dimeric protein with two-state characteristics obeys different thermodynamic and kinetic laws. The unfolding and refolding reactions differ mechanistically, the former being unimolecular, the latter bimolecular (*26*). Thus, the rates for the two reactions at a certain GdmCl concentration are no longer equal (cf. eq 13).

Two-State Folding. Figure 1A shows the equilibrium transition at 15 °C measured by three different structural probes. The native state unfolds and dissociates in a highly cooperative manner; all spectroscopic signals coincide. Fluorescence and CD spectra have common isofluorescent and isodichroic points throughout the whole transition (430 and 211 nm, respectively). The transition range is very narrow; no intermediates can be detected. The dimeric species in the predenaturation range not only display spectroscopic identity with the native state but also has the same stability; their unfolding kinetics have the same rate constants as the native state, even in the transition range itself (Figure 1B). Similarly, the unfolded monomeric protein at GdmCl concentrations beyond 2.5 M shows identical spectral properties and the same refolding behavior, again reaching into the transition range. From the change in the extinction coefficients of the unfolded and native species, the exposure of one Trp residue per subunit is determined (cf. Materials and Methods). As TmDHFR contains one Trp per monomer in the hydrophobic environment of the active site, this result clearly indicates disruption of the core of the enzyme. Accordingly, as there are only two species populated at

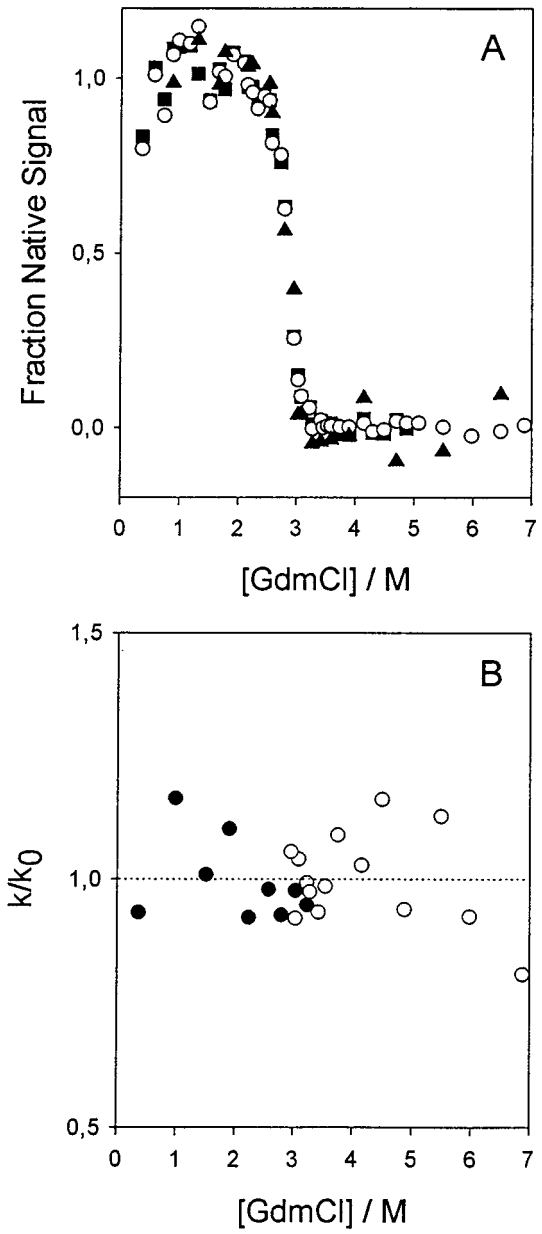

FIGURE 1: Equilibrium renaturation transition of TmDHFR at 15 °C. Protein concentration: 5.2 μM. (A) Normalized signals of ellipticity at 222 nm (○), fluorescence emission at 330 nm after excitation at 280 nm (■), absorption at 288 nm (▲). (B) Rate constants of unfolding in 7.2 M GdmCl (●) and refolding in 0.34 M GdmCl (○) of the equilibrium species in (A), normalized to the value for native or denatured TmDHFR.

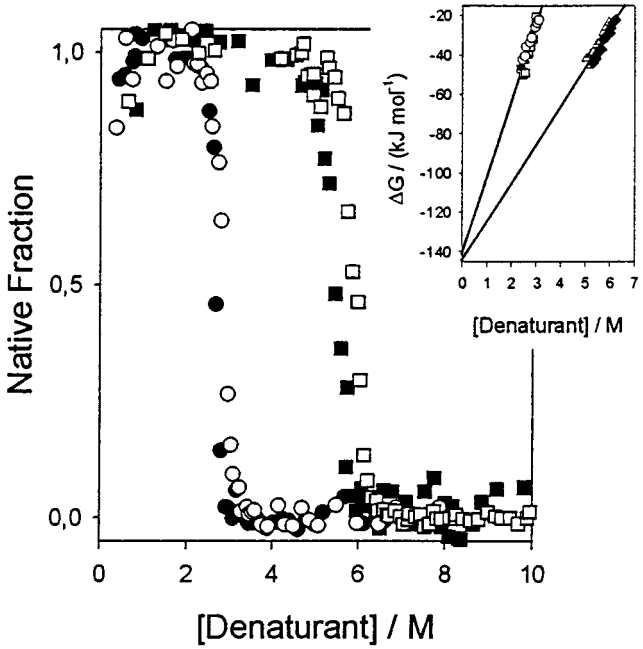

FIGURE 2: Equilibrium transition of TmDHFR at 15 °C and varying protein concentrations. Normalized signals of native fluorescence emission. GdmCl-induced transition at a protein concentration P_t = 0.52 (●) and 5.2 μM (○). Urea-induced transition at P_t = 0.4 (■) and 4 (□) μM. Insert: Linear extrapolation of ΔG in the transition region to zero denaturant concentration; ΔG determined from eq 2−5. Protein concentration: 0.1 (○), 0.5 (△) and 5 (□) μM in GdmCl; 0.4 (▲) and 4 (◆) μM in urea.

Table 2: Thermodynamic Parameters of TmDHFR Unfolding at Different Temperatures; Protein Concentration P_t = 0.52 μM

T (°C)	denaturant	$C_{1/2}$ (M)	m [kJ/(mol·M)]	ΔG_{H2O} (kJ/mol)	$\Delta G_{2.9M}$ (kJ/mol)[a]
5	GdmCl	2.23	55.4	−155.5	2.9
15	GdmCl	2.75	39.3	−141.0	−28.6
15[b]	GdmCl	2.85[b]	39.3	−141.0	−28.6
15	urea	5.45	19.7	−144.4	−
25	GdmCl	3.07	29.9	−125.9	−40.5
37	GdmCl	3.36	25.0	−118.5	−48.2
55	GdmCl	3.01	26.1	−116.2	−41.5
55[b]	GdmCl	3.21[b]	n.d.	n.d.	n.d.
70	GdmCl	2.38	31.6	−114.3	−24.1
error[c] (%)		−	10	20	10

[a] Calculated from eq 5. [b] Protein concentration: P_t = 5.2 μM. [c] Errors were estimated by variation of base lines and multiple measurements.

equilibrium, the native dimer and the unfolded monomer (Table 1), the folding follows the two-state model for a dimeric protein: $N_2 \rightleftarrows 2U$.

Since equilibria obey the law of mass action, they are influenced by the concentration of the protein, higher concentration favoring the dimeric native state (*21*). Due to the high cooperativity of the transition, this effect is hardly detectable in strong denaturants such as GdmCl, but obvious in a weaker denaturant such as urea (Figure 2). As one can easily see from eq 10, this behavior is what one would predict (*22*):

$$C_{1/2} = -\left[\ln (2P_t) + \frac{\Delta G}{RT}\right]\frac{RT}{m} \qquad (10)$$

with $C_{1/2}$ the concentration of the transition midpoint. Equilibrium constants and free energies of stabilization can be determined for the transition range, making use of eq 4. From the linear extrapolation to zero denaturant concentration (*27*), ΔG_{H2O} can be determined (insert, Figure 2). The linear extrapolation for GdmCl and urea yields the same value for ΔG_{H2O}. The resulting free energies of stabilization (Table 2) represent the highest values observed so far for a dimeric protein. The corresponing cooperativity (m-value) is slightly larger than the value expected for a protein of the given size (*28*), providing further support for the two-state model: if intermediates were present at equilibrium, the m-values would decrease significantly (*20*).

The equal population of native dimer and unfolded monomer at the transition midpoint is verified by sedimentation analysis in the analytical ultracentrifuge close to the

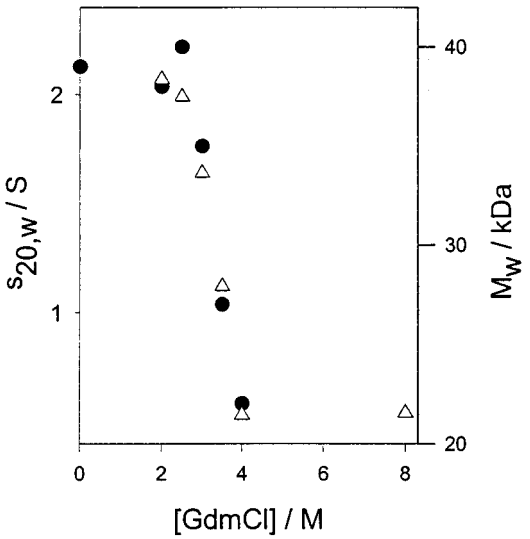

FIGURE 3: Analytical ultracentrifugation of TmDHFR. Protein concentration $P_t = 26$ μM, 20 °C. GdmCl-induced equilibrium transition recorded by molecular mass M_w (●) and sedimentation coefficient $s_{20,w}$ (△).

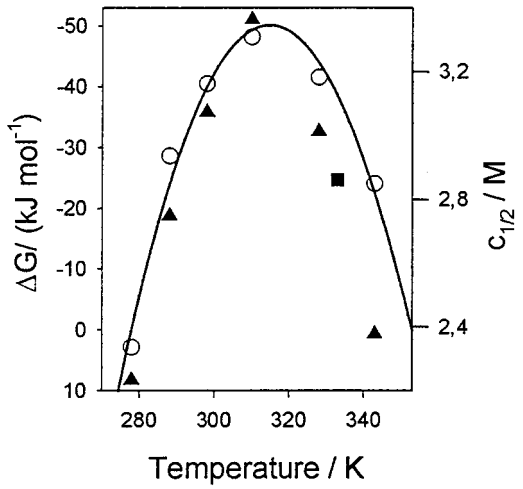

FIGURE 4: Thermodynamic stability of TmDHFR in 2.9 M GdmCl. (○) $\Delta G_{2.9M\ GdmCl}$ from Table 2; solid line, plot of eq 11 with the following parameters: $\Delta H_m = -466$ kJ/mol, $T_m = 333$ K, $\Delta C_p = 22.4$ kJ/(mol·K), $P_t = 5 \times 10^{-7}$ M. (▲) Denaturant concentration of half-denaturation; (■) melting point at 2.9 M GdmCl from eq 11.

transition midpoint (Figure 3). The data at 3.5 M GdmCl can be described by the presence of two distinct species with an association equilibrium constant $K_a \approx 1$ M. From this result, it follows that the concentrations of the unfolded species must be close to the square root of the concentration of the native species ([U] $\approx \sqrt{[N_2]}$).

Stability Profile. To determine further thermodynamic parameters for the folding−unfolding reaction, the temperature dependence of the free energy of stabilization was determined at 5−70 °C. Over this whole temperature range, the two-state assumption is found to be valid. Evidence is taken from the following three observations: (i) the unfolding and refolding transitions match after sufficiently long time; (ii) different spectroscopic signals in the GdmCl-induced transition coincide; and (iii) cooperativity is high over the whole temperature range. The midpoint of the transition depends on the protein concentration; the respective shift of $C_{1/2}$ is significantly more pronounced at higher temperatures due to the decrease in cooperativity, as predicited by eq 10 (Table 2). Due to interactions with the walls of the cuvettes, the pre-transitional base line is more difficult to determine at increased temperatures. By manually varying the pre-transitional base lines, the error in ΔG_{H2O} introduced by this uncertainty can be examined. Due to the extrapolation over large differences in denaturation concentration, the error in the *m*-values affects ΔG_{H2O} significantly (see Table 2). Since the transition midpoints at different temperatures cluster at a GdmCl concentration of 2.9 M, the error is minimized by calculating ΔG at 2.9 M GdmCl (*29*).

The stability profile in the presence of 2.9 M GdmCl (Figure 4) displays a maximum at around 35 °C, both for ΔG and for $C_{1/2}$; i.e., below this temperature, cold destabilization occurs. The curve is described by the usual expression for a stability curve of a dimeric protein:

$$\Delta G = RT \ln (2P_t) - \Delta H_m\left(1 - \frac{T}{T_m}\right) - \Delta C_p\left(T - T_m - T \ln \frac{T}{T_m}\right) \quad (11)$$

with ΔH_m the enthalpy of melting, T_m the melting temperature, and ΔC_p the change in heat capacitiy between the native and the unfolded states (*30*, *31*). At a protein concentration $P_t = 0.52$ μM, the fit of eq 11 to the data in Figure 4 yields the midpoint of the melting transition at 333 K for 2.9 M GdmCl, in agreement with the experimental $C_{1/2}$ vs T profile (Figure 4). The latter profile is also parabolic; however, no fit has been attempted because of the accumulation of the errors in $C_{1/2}$ and *m*. For a protein the size of TmDHFR, ΔC_p is expected to be ca. 23 kJ/(mol·K) (*28*); this is confirmed by the value 22.4 kJ/(mol·K) used to fit the stability profile.

Unfolding Kinetics. Folding and unfolding kinetics were performed at 15 °C, i.e., under the same conditions used previously for studies on the enzyme from *E. coli* (EcDHFR) (*6*). Thus, given the structural homology of the two enzymes, the kinetic data can be compared. However, previous results have shown that the biophysical characteristics of hyperthermophilic and mesophilic proteins converge under their respective physiological conditions (*2*, *4*). This concept of "corresponding states" would imply that the physical parameters of the enzyme from *T. maritima* (optimum growth temperature $T_{opt} = 80$ °C) at 55 °C should be close to those of EcDHFR at 15 °C.

The signal amplitude of the unfolding reactions at different temperatures and denaturant concentrations beyond 6 M GdmCl accounts for the total change in signal (Figure 5A). Thus, there are no undetected phases in the dead-time of the mixing experiment. The progress curves can be described by a single exponential (eq 6), and the rate constants are identical for the different spectroscopic signals (Figure 5B). Obviously, unfolding proceeds in a single step without the occurrence of intermediates. Beyond 6 M GdmCl, the rate constants are found to be independent of protein concentration over a 50-fold concentration range. Because of the extremely slow unfolding reactions at 15 °C, no measurements were performed below 6 M GdmCl; at 55 °C, denaturation kinetics were followed over the whole transition range. Below 5.5 M GdmCl, at 55 °C, the unfolding reaction deviates from a single-exponential decay. The time course

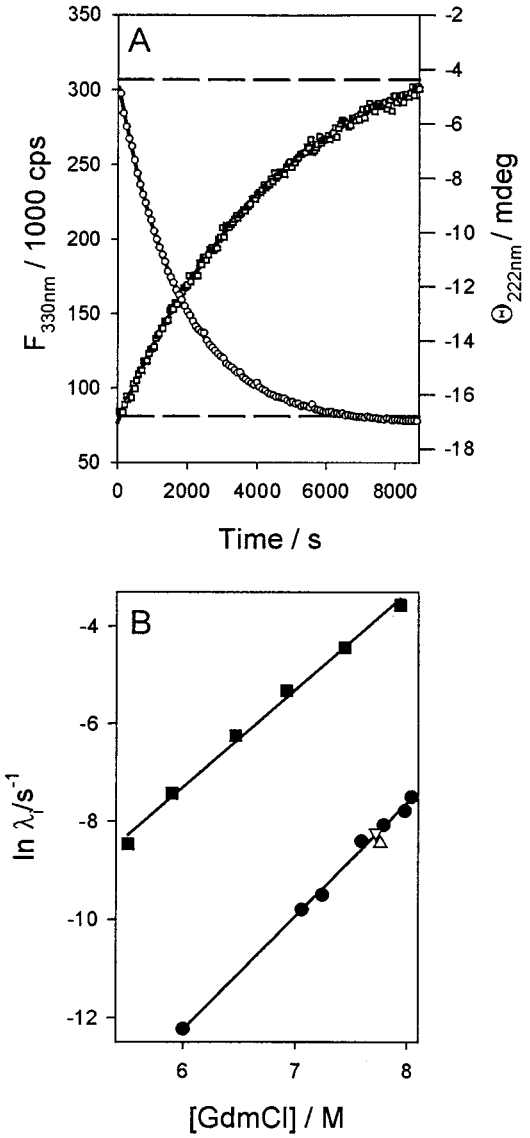

FIGURE 5: Unfolding kinetics. (A) At 15 °C monitored as the change in native fluorescence (○) in 8 M GdmCl, protein concentration $P_t = 0.52\ \mu$M; change in native ellipticity (□) in 7.8 M GdmCl, protein concentration $P_t = 5.2\ \mu$M. Solid lines: fit to eq 6 with $i = 1$; the fit matches the experimental data perfectly. Dashed lines: values extrapolated from equilibrium transitions using the signals of the native and unfolded states. (B) Dependencies of the rate constants of unfolding on denaturant concentration and temperature, monitored by the decrease of native fluorescence at 15 (●) and 55 °C (■). Solid line: linear fit. (△) Unfolding rate from ellipticity at 222 nm. (▽) U → N → U double jump: unfolding rate of renatured TmDHFR monitored immediately after the spectroscopic plateau value was reached.

depends now on the protein concentration, proving that the backward bimolecular reaction becomes significant. For the simple case of a bimolecular association reaction

$$N_2 \underset{k_f}{\overset{k_u}{\rightleftharpoons}} 2U \tag{12a}$$

or in differential form:

$$d[U]/dt = -k_f[U]^2 + 2k_u[N_2] \tag{12b}$$

the time course of unfolding is described by a single exponential only far away from equilibrium, i.e., for $k_f \ll k_u$. As has been mentioned, this condition holds true for GdmCl concentrations ≥6 M, where the observed time constants λ_i equal $2k_u$. Figure 5B shows the increase in reaction rate with increasing denaturant concentration, and allows the kinetic *m*-values m_u to be calculated: for 15 and 55 °C, the results are −5528 and −5424 J/(mol·M), respectively, accounting for 14% and 20% of the equilibrium *m*-value (cf. Table 2). Explaining the *m*-values in terms of interactions of the denaturant with either the transition state or the unfolded state of the protein (*32*), it follows that over the given temperature range, the accessibility of the transition state of the protein for GdmCl is much closer to the native than to the unfolded state. Extrapolating the rate constants for unfolding to zero denaturant concentration (Figure 5B), k_u at 15 °C is found to be 4.6×10^{-12} s^{-1}, which differs from the value determined for the slowest unfolding phase of EcDHFR (*6*) by 8 orders of magnitude. Even at 55 °C, the unfolding of TmDHFR is slower than that of EcDHFR at 15 °C by a factor of 10^5 ($2k_u = 4.4 \times 10^{-9}$ s^{-1}). Obviously, the concept of corresponding states does not apply here, at least not to the unfolding kinetics.

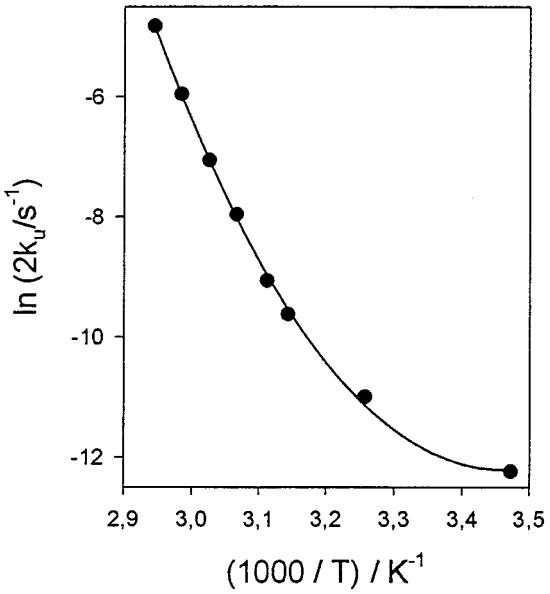

FIGURE 6: Temperature dependence of unfolding rate constants in 6 M GdmCl (●), plotted as Arrhenius diagram. Solid line: plot of eq 9 with the following parameters: $\Delta H^{\ddagger}_{25°C} = 42$ kJ/mol, $\Delta S^{\ddagger}_{25°C} = -202$ J/(mol·K), $\Delta C_p^{\ddagger} = 4.9$ kJ/(mol·K).

Temperature Dependence of Unfolding. Given the fact, that at 6 M GdmCl the measured rate constant λ_i equals $2k_u$, the temperature dependence of the unfolding rate constant could be determined between 15 and 66 °C (Figure 6). The resulting curved Arrhenius plot may be attributed to a positive $\Delta C_p^{\ddagger}$ of 4932 J/(mol·K), which implies, that in approaching the transition state of unfolding, additional surface becomes exposed to the solvent. The ratio of $\Delta C_p^{\ddagger}$ and the total change in heat capacity from the equilibrium transition is ≈22%, again indicating that the transition state is nativelike. The activation enthalpy of this reaction, $\Delta H^{\ddagger}_{25°C} = 42.4$ kJ/mol, is positive; i.e., energy is needed to produce the partially disrupted bonds of the transition state (*33*). The activation entropy, $\Delta S^{\ddagger}_{25°C} = -201.7$ J/(mol·K), is negative, which can be interpreted as entropic cost for ordering of denaturant and/or water molecules around the protein in its

transition state (*34*). $\Delta S^{\ddagger}$ changes its sign at 37 °C, coinciding with the point of maximum stability.

Refolding Kinetics. Given the equilibrium constant K and the unfolding rate constant k_u at varying GdmCl concentration (cf. eqs 5 and 7), the rate constant for the bimolecular refolding process k_f can be calculated from

$$K_u = 2k_u/k_f \tag{13}$$

(*26*). Obviously, the figure at 0 M GdmCl, $k_f = 3.6 \times 10^{14}$ s^{-1} M^{-1}, is unrealistically large because 10^9 s^{-1} M^{-1} would be the limiting rate of a diffusion-controlled reaction. Thus, in the absence of denaturant, the association of the monomers cannot be rate-limiting. At 2 M GdmCl, the calculated rate constant ($k_f = 198$ s^{-1} M^{-1}) indicates, that close to the denaturation midpoint, the bimolecular process becomes rate-limiting according to

$$A(t) = A_0 + \Delta A\left(\frac{[P]k_f t}{1 + [P]k_f t}\right) \tag{14}$$

with A the signal at time t, A_0 the signal of the unfolded state, ΔA the signal difference to the native state, k_f the bimolecular rate constant, and [P] the protein concentration (*26*). Figure 7 illustrates the simulated kinetics of the bimolecular reaction at low GdmCl concentration and close to the transition midpoint. Below 1.8 M GdmCl, the association cannot be rate-limiting, as all observed kinetics proceed much slower than the simulated curve. The measured kinetics are independent of the concentration of the protein and can be described by the sum of two exponential functions and a dead-time amplitude; they cannot be fitted by eq 14. Thus, the observed refolding processes must be unimolecular reactions, either preceding or following the fast association step. At 2 M GdmCl, however, the simulated curve for a simple association reaction is slower than the observed kinetics, suggesting that under this condition, a bimolecular process dominates. In fact, the mechanism is more complex because, despite a significant concentration dependence of the kinetics, the overall reaction still fits a single exponential, except for the early phase of the reaction (Figure 6B). It is mainly this phase which is affected by varying the protein concentration. Even for the simplest case of an irreversible uni-bimolecular folding reaction, the rate equations are complex (*35*). The folding kinetics of TmDHFR are surely more complicated since there are at least two further intermediates involved (see below). Therefore, no general mathematical representation of the refolding kinetics close to equilibrium is attempted. Still, the fact that the deviations of the folding process from unimolecular kinetics occur precisely at the GdmCl concentration predicted by the simulations proves that the extrapolations of K and k_u must be valid: The model correctly predicts the observed behavior.

As shown in Figure 8A, two exponential terms plus a dead-time amplitude are required to describe both the changes in fluorescence emission and the far-UV CD signal adequately. There is no improvement of the fits if a third exponential is included. The dead-time amplitude ($\tau < 10$ s) amounts to $\leq$20% of the total signal change, which means that reactions during the burst phase do not result in significant structure formation in comparison with the overall recovery of the native state. Immediately after reaching the spectral characteristics of native TmDHFR, the refolded enzyme exhibits full stability: the unfolding kinetics of the protein right after reaching the native fluorescence and CD signals are exactly the same as observed for the native enzyme (cf. U → N → U double jump in Figure 5B). This observation proves that the reactions involved in the whole unfolding/refolding cycle are complete.

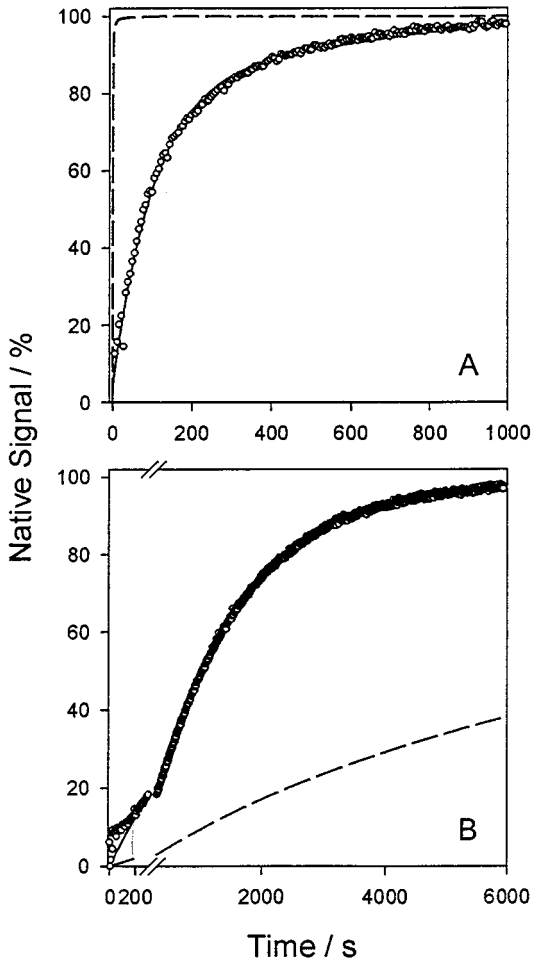

FIGURE 7: Refolding kinetics of TmDHFR ($P_t = 0.52$ μM, 15 °C) monitored by native fluorescence (○). (A) In 1.24 M GdmCl; (B) in 2 M GdmCl. Solid line: fit to eq 6 with $i = 2$ (A) or $i = 1$ (B). In (B), the fit beyond 200 s matches the experimental data. Dashed line: expected time course for a bimolecular reaction simulated using eq 14, and a folding rate constant calculated from eq 13; protein concentration $P_t = 0.52$ μM.

Figure 8B summarizes the rate constants observed for the unimolecular folding processes at varying GdmCl concentration. Independent of the method (fluorescence or far-UV CD), the observed reaction rates are the same. Folding is a highly cooperative process, with simultaneous formation of secondary and tertiary structures. This is not only true for the burst phase, but also for subsequent intermediates. For the faster phase, the relative amplitudes of the spectral changes are 64 ± 13% (monitored by fluorescence) and 60 ± 8% (monitored by far-UV CD). At 15 °C, both phases of the renaturation reaction depend on the denaturant concentration. Although a description of the folding kinetics in 2 M GdmCl with one single exponential is not fully adequate for the early phases (see above), the rate constant for the slow

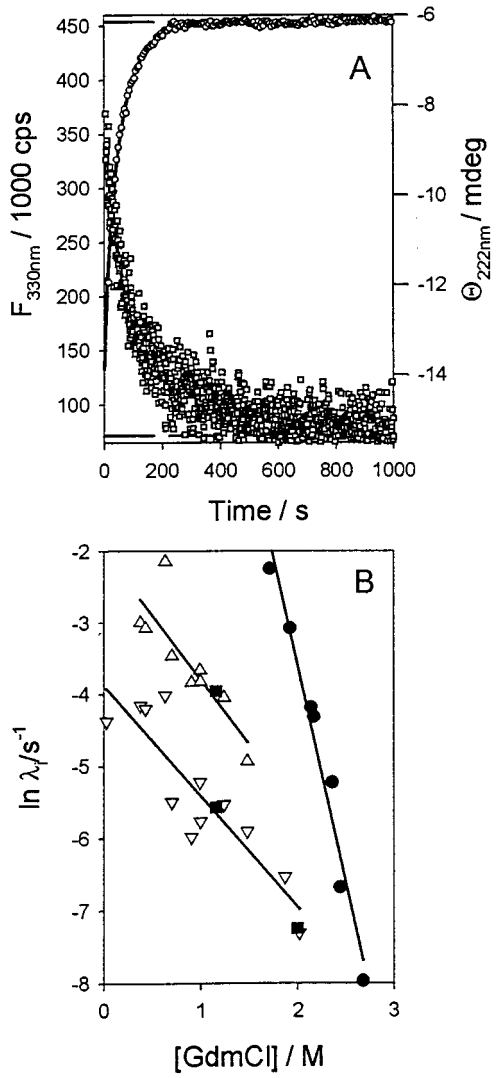

FIGURE 8: Refolding kinetics. (A) At 15 °C monitored by the regain of native fluorescence (○) in 0.43 M GdmCl (protein concentration: $P_t = 0.52$ μM) and by the change in native ellipticity (□) in 1.16 M GdmCl (protein concentration: $P_t = 5.2$ μM). Solid lines: fit to eq 6 with $i = 2$. Dashed lines: value extrapolated from equilibrium transitions using the signals of the native and unfolded states. (B) Dependence of the refolding rate constants at 15 °C from fluorescence kinetics (fast phase, △; slow phase, ▽), and from CD kinetics at 222 nm (■); 55 °C, only fluorescence kinetics (●). Solid lines represent linearizations yielding the following kinetic *m*-values: for 15 °C, −4.3 kJ/(mol·M) (for the fast phase) and −3.6 kJ/(mol·M) (for the slow phase); for 55 °C, −14.4 kJ/(mol·M).

reaction still fits the linear concentration dependence of the slow reaction at ≤1.8 M GdmCl.

At 55 °C, only a single phase is detected, which is more dependent on denaturant concentration than the two phases at 15 °C. An estimate of the burst phase amplitude again yields ca. 20%, but due to the difficulty in determining native base lines at high temperatures, no exact value can be given. Still, that phase is rather low in amplitude, analogous to the finding at the lower temperature. A treatment of the renaturation reaction at 55 °C, similar to the one presented in Figure 7, suggests that the association reaction becomes rate-limiting only beyond 2.5 M GdmCl. Accordingly, progress curves should follow unimolecular kinetics below 2.5 M GdmCl; this is exactly what is observed. Kinetics in GdmCl concentrations below 1.9 M are too fast to be measured by the manual mixing technique.

DISCUSSION

Two-State Model. Considering the small size of its polypeptide chains (168 amino acid residues per subunit), TmDHFR shows anomalously high intrinsic stability. The present data give a full thermodynamic and kinetic description of the ultrastable homodimeric protein, showing that the $N_2 \rightleftarrows 2U$ two-state model of folding is sufficient to interpret the equilibrium data. Under no condition can structured monomers be observed; breaking the intersubunit contacts destroys the integrity of the constituent parts of the dimer. This is in line with the general observation that protein folding and association are highly cooperative "all or none" processes. This holds especially for TmDHFR in which the subunit interactions involve a relatively large surface area with numerous amino acid residues in close contact. Preliminary data from high-resolution X-ray crystallography clearly show that the last two β-strands of each monomer are involved in an extended contact area along the full length of both structural elements. The overall fold is conserved. Refinement of both the apo-enzyme and the complex with methotrexate and NADPH is in progress (T. Dams, G. Auerbach, G. Bader, R. Jaenicke, and R. Huber, in preparation).

In comparing monomeric and oligomeric proteins, one has to keep in mind that numerical values of ΔG_{H2O} cannot be used directly as a quantitative measure of protein stability. In eq 4, 1 M standard concentrations of all reactants were assumed. Depending on the normalization, different values for ΔG_{H2O} are obtained; this is reflected by the fact that ΔG is not equal to zero at the transition midpoint. For monomeric proteins, no such normalization is required in order to calculate the stability. In the case of dimeric proteins, commonly the normalization refers to 1 molar concentrations, this way allowing the comparison of various dimeric systems. In the case of DHFR, no ΔG data for mesophilic dimers are known. Thus, the change in the free energy, $\Delta\Delta G_{H2O}$, in going from mesophilic to hyperthermophilic DHFRs cannot be given. The stability of an isolated monomer cannot be determined, since no monomeric intermediates are detectable at equilibrium in accordance with the two-state model: any condition causing dissociation of the native state also leads to unfolding of the subunits (*13*, *36*). Still, the association cannot be the only stabilizing principle for several reasons: (i) At present, at least two dimeric DHFRs of mesophilic origin are known (*14*, *15*). (ii) Folding and association must necessarily involve monomeric intermediates. Since in vitro denaturation is fully reversible, even at high temperatures, the monomeric intermediates must be stable and nativelike in order to dimerize rather than aggregate (*37*). (iii) Although the measured stability cannot be separated into contributions from monomer folding and dimer association, the observed high Gibbs free energy of stabilization cannot originate from dimerization alone; it must also comprise the intrinsic stability of the contributing monomers.

Several examples of anomalously high states of association for hyperthermophilic proteins have been reported in the past (*4*). On the other hand, there are several examples that clearly contradict a generalization: enolase from *Pyrococcus furiosus* is a dimer (*38*), whereas most mesophilic enolases are octamers; octameric lactate dehydrogenase (LDH) from *T. maritima* does not show higher stability than the tetrameric

form (*39*); *T. neapolitana* xylose isomerase is equally stable in both the tetrameric and the dimeric state (*40*). The tetrameric LDH from *Bacillus stearothermophilus* is converted into a thermostable dimer by site-directed mutagenesis (*41*). The question is still open, to what extent additional quaternary interactions are involved in the stabilization of hyperthermophilic proteins. With the high-resolution X-ray structure in our hands, specific mutations in the contact surface may help to clarify their importance.

Stability Profile. The two-state model has been shown to be valid over the whole temperature range from 5 to 70 °C. The temperature dependence of the thermodynamic equilibrium allows specific adaptative mechanisms of the hyperthermostable protein to be investigated. According to (*42*), a more or less parabolic temperature profile of protein stability can be deduced from the assumption of a constant change in heat capacity upon unfolding. It is determined by the melting point T_m, the melting enthalpy ΔH_m, and the change in heat capacity ΔC_p. For most mesophilic proteins, it displays its maximum at a relatively low temperature, often below the freezing point of water.

In principle, hyperthermophilic proteins can adapt toward the dissipative action of thermal energy either by shifting the maximum of the profile toward higher temperature or by lifting the optimum stability to a higher ΔG level, or simply by increasing the stability range by flattening the parabola; evidently, combinations of the three alternatives are also possible (*1*, *4*, *43*). In the case of TmDHFR, the stability curve represents a combination of the first and second alternatives: The parabola is lifted to a higher ΔG level, and its optimum is shifted to a higher temperature (the maximum value observed for a dimeric protein so far); no flattening is detectable. Flattening would reflect a change in heat capacity which is known to be correlated with the excess surface area that is exposed to the solvent upon unfolding. This area depends on the size of the protein. Using parameters reported for monomeric and multimeric proteins (*28*), the change in heat capacity for the unfolding of TmDHFR is expected to be ca. 23 kJ/(mol·K), in accordance with the observed value. As this result was obtained in the presence of denaturant, GdmCl binding may cause a slight decrease of ΔC_p (*44*−*47*). The variation of equilibrium *m*-values with temperature also reflects protein−denaturant interactions. However, as the change in *m* is within the range of error, the correction in ΔC_p cannot be significant (*31*, *46*, *48*).

Mechanism of Unfolding and Refolding. The unfolding reaction of TmDHFR over a wide temperature range is determined by one single unimolecular kinetic phase. In contrast to the enzyme from *E. coli* and *Lactobacillus casei*, there is no evidence for multiple native substates in the case of TmDHFR (*6*, *49*), despite forming a stable dimer and sharing exceedingly higher intrinsic stability compared to its mesophilic homologues. It is worth mentioning, that even at high temperature, the unfolding of TmDHFR is slow compared to the "corresponding state" of EcDHFR; obviously, the hyperthermophilic protein displays high kinetic stability.

Kinetic studies allow the thermodynamic stability to be dissected into the contributions of the forward and the backward reaction, eventually giving further insight into the stabilizing principles. The shift in the equilibrium toward the native state has often been shown to be attributable to a decrease in the unfolding rate, rather than an increase in the refolding rate (*24*, *50*, *51*). Considering its drastically decreased unfolding rate compared to mesophilic DHFRs, this strategy is clearly valid for the hyperthermophilic TmDHFR. Still, the transition state is close to the native state on the reaction coordinate, which means that the essential stabilizing interactions must be formed late on the folding pathway (*51*). As has been shown, the unfolding kinetics are not concentration dependent. Thus, the transition state may be assumed to be the dimer with perturbed subunit interactions, which would imply that dimerization cannot be the only stabilizing principle.

The refolding reaction is difficult to interpret in terms of a specific mechanism of adaptation toward high temperatures. As has been shown, reversibility is maintained up to 70 °C, and no help of molecular chaperones is needed. These two findings clearly imply that intermediates on the pathway of folding and association must be resistant toward irreversible side reactions; i.e., they must exhibit high intrinsic stability, both at the monomer and at the dimer level. No direct comparison with defined folding phases for EcDHFR is attempted because of the fundamental difference in the quaternary structure of both enzymes. For the overall reaction, it is interesting to note that the order of magnitude of the folding rates is the same, in contrast to the unfolding reaction, which shows the characteristics of kinetic stabilization (*50*). In the case of the two phases observed at low temperature (15 °C), it remains unclear whether consecutive or parallel reactions are involved. Early short-lived intermediates were experimentally inaccessible with the methods applied. As taken from the amplitudes observed by fluorescence and CD, these reactions do not contribute to extended structure formation. Dimerization does not represent a rate-limiting step in the overall folding/association mechanism. Evidently, the reaction is fast compared to preceding or subsequent rearrangements of the tertiary and quaternary structure. One may assume, that this also holds in vivo, where the concentration of the enzyme is significantly lower than the concentration in most of the present in vitro reconstitution experiments.

ACKNOWLEDGMENT

We thank Drs. W. Pfeil, F. X. Schmid, H. Schurig, K. Zaiss, D. Wassenberg, C. Welker, M. Kretschmar, and R. Thoma for fruitful discussions and G. Pappenberger for critically reading the manuscript. The generous support of Professor R. Huber, Dr. G. Auerbach, G. Bader, and T. Ploom in the structure determination and the excellent technical assistance of Barbara Kellerer are gratefully acknowledged.

REFERENCES

1. Jaenicke, R., Schurig, H., Beaucamp, N., and Ostendorp, R. (1996) *Adv. Protein Chem. 48*, 181−269.
2. Jaenicke, R. (1991) *Eur. J. Biochem. 202*, 715−728.
3. Rehaber, V., and Jaenicke, R. (1992) *J. Biol. Chem. 267*, 10999−11006.
4. Jaenicke, R., and Böhm, G. (1998) *Curr. Opin. Struct. Biol. 8*, 738−748.
5. Sawaya, M. R., and Kraut, J. (1997) *Biochemistry 36*, 586−603.

6. Touchette, N. A., Perry, K. M., and Matthews, C. R. (1986) *Biochemistry 25*, 5445−5452.
7. Jones, B. E., Beechem, J. M., and Matthews, C. R. (1995) *Biochemistry 34*, 1867−1877.
8. Hoeltzli, S. D., and Frieden, C. (1998) *Biochemistry 37*, 387−398.
9. Vestweber, D., and Schatz, G. (1988) *EMBO J. 7*, 1147−1151.
10. Viitanen, P. V., Donaldson, G. K., Lorimer, G. H., Lubben, T. H., and Gatenby, A. A. (1991) *Biochemistry 30*, 9716−9723.
11. Goldberg, M. S., Zhang, J., Sondek, S., Matthews, C. R., Fox, R. O., and Horwich, A. L. (1997) *Proc. Natl. Acad. Sci. U.S.A. 94*, 1080−1085.
12. Koehler, C. M., Farosch, E., Tokatlidis, K., Schmid, K., Schweyen, R. J., and Schatz, G. (1998) *Science 279*, 369−373.
13. Dams, T., Böhm, G., Auerbach, G., Bader, G., Schurig, H., and Jaenicke, R. (1998) *Biol. Chem. 379*, 367−371.
14. Purohit, S., Bestwick, R. K., Lasser, G. W., Rogers, C. M., and Mathews, C. K. (1981) *J. Biol. Chem. 256*, 9121−9125.
15. Novak, P., Stone, D., and Burchall, J. J. (1983) *J. Biol. Chem. 258*, 10956−10959.
16. Wilquet, V., Gaspar, J. A., van de Lande, M., van de Casteele, M., Legrain, C., Meiering, E. M., and Glansdorff, N. (1998) *Eur. J. Biochem. 255*, 628−637.
17. Donovan, J. W. (1973) *Methods Enzymol. 27*, 497−525.
18. Yphantis, D. A. (1964) *Biochemistry 3*, 297−317.
19. Durchschlag, H., and Jaenicke, R. (1982) *Biochem. Biophys. Res. Commun. 108*, 1074−1079.
20. Pace, C. N. (1986) *Methods Enzymol. 131*, 266−280.
21. Neet, K. E., and Timm, D. E. (1994) *Protein Sci. 3*, 2167−2174.
22. Backes, H., Berens, C., Helbl, V., Walter, S., Schmid, F. X., and Hillen, W. (1997) *Biochemistry 36*, 5311−5322.
23. Eyring, H. (1935) *J. Chem. Phys. 3*, 107−115.
24. Cavagnero, S., Debe, D. A., Zhou, Z. H., Adams, M. W. W., and Chan, S. I. (1998) *Biochemistry 37*, 3369−3376.
25. Jaenicke, R., and Rudoph, R. (1986) *Methods Enzymol. 131*, 218−250.
26. Milla, M. E., and Sauer, R. T. (1994) *Biochemistry 33*, 1125−1133.
27. Greene, R. F., and Pace, C. N. (1974) *J. Biol. Chem. 249*, 336−348.
28. Myers, J. K., Pace, C. N., and Scholtz, J. M. (1995) *Protein Sci. 4*, 2138−2148.
29. Goldenberg, D. P. (1992) in *Protein Folding* (Creighton, T. E., Ed.) pp 353−403, W. H. Freeman & Co., New York.
30. Steif, C., Weber, P., Hinz, H. J., Flossdorf, J., Cesareni, G., and Kokkinidis, M (1993) *Biochemistry 32*, 3867−3876.
31. Backmann, J., Schäfer, G., Wyns, L., and Bönisch, H. (1998) *J. Mol. Biol. 284*, 817−833.
32. Shortle, D. (1995) *Adv. Protein Chem. 46*, 217−247.
33. Oliveberg, M., Tan, Y., and Fersht, A. R. (1995) *Proc. Natl. Acad. Sci. U.S.A. 92*, 8926−8929.
34. Chen, X., and Matthews, C. R. (1994) *Biochemistry 33*, 6356−6362.
35. Chien, J. Y. (1948) *J. Am. Chem. Soc. 70*, 2256−2261.
36. Dams, T. (1998) Ph.D. Thesis, University of Regensburg.
37. Jaenicke, R., and Seckler, R. (1997) *Adv. Protein Chem. 50*, 1−59.
38. Peak, M. J., Peak, J. G., Stevens, F. J., Blamey, J., Mai, X., Zhou, Z. H., and Adams, M. W. W. (1994) *Arch. Biochem. Biophys. 313*, 280−286.
39. Dams, T., Ostendorp, R., Ott, M., Rutkat, K., and Jaenicke, R. (1996) *Eur. J. Biochem. 240*, 274−279.
40. Hess, J. M., Tchernajenko, V., Vielle, C., Zeikus, J. G., and Kelly, R. M. (1998) *Appl. Eviron. Microbiol. 64*, 2357−2360.
41. Jackson, R. M., Gelpi, J. L., Cortes, A., Emery, D. C., Wilks, H. M., Moreton, K. M., Halsall, D. J., Sleigh, R. N., Behan-Martin, M., Jones, G. R., Clarke, A. R., and Holbrook, J. J. (1992) *Biochemistry 31*, 8307−8314.
42. Becktel, W. J., and Schellman, J. A. (1987) *Biopolymers 26*, 1859−1877.
43. Jaenicke, R., and Böhm, G. (1999) *Methods Enzymol.*, Vol. Hyperthermophilic Enzymes (in press).
44. Chen, B. L., and Schellman, J. A. (1989) *Biochemistry 28*, 685−691.
45. Makhatadze, G. I., and Privalov, P. L. (1992) *J. Mol. Biol. 226*, 491−505.
46. Agashe, V. R., and Ugdaonkar, J. B. (1995) *Biochemistry 34*, 3286−3299.
47. Schellman, J. A., and Gassner, N. C. (1996) *Biophys. Chem. 59*, 259−275.
48. Chiti, F., van Nuland, N. A. J., Taddei, N., Magherini, F., Stefani, M., Ramponi, G., and Dobson, C. M. (1998) *Biochemistry 37*, 1447−1455.
49. Falzone, C. J., Wright, P. E., and Benkovic, S. J. (1991) *Biochemistry 30*, 2184−2191.
50. Pappenberger, G., Schurig, H., and Jaenicke, R. (1997) *J. Mol. Biol. 274*, 676−683.
51. Perl, D., Welker, C., Schindler, T., Schröder, K., Marahiel, M. A., Jaenicke, R., and Schmid, F. X. (1998) *Nat. Struct. Biol. 5*, 229−235.

BI990635E